

**Moment tensor inversion of the spectral amplitude of mantle surface waves:  
Toward realistic real-time focal solutions based on very small datasets**

*Dominique Reymond*

*CEA, DASE, Laboratoire de Géophysique, BP 640  
F – 98713 Papeete, Tahiti, French Polynesia*

*e-mail: reymond@labogeo.pf*

*Emile A. Okal*

*Department of Geological Sciences, Northwestern University  
Evanston, IL 60208, USA*

*e-mail: emile@earth.nwu.edu*

**Presentation made at the International Conference  
on Tsunamis  
Paris – May 26 to 28, 1998**

**Moment tensor inversion of the spectral amplitude of mantle surface waves:  
Toward realistic real-time focal solutions based on very small datasets**

*Dominique Reymond, CEA, DASE, Laboratoire de Géophysique, BP 640,  
F-98713 Papeete, Tahiti, French Polynesia,*

*Emile A. Okal, Department of Geological Sciences, Northwestern University,  
Evanston, IL 60208, USA.*

**Abstract**

Recent improvements in automated data processing and satellite communications make it feasible to estimate in quasi real time the focal parameters of a distant earthquake, including depth and moment tensor components. Our procedure is oriented toward strong events in the context of tsunami warning. We adapt the formalism of Romanovicz and Suárez [1983] to the case of very small datasets involving as few as three stations. The data consist of the amplitude spectra of mantle surface waves, transmitted automatically by satellite via INMARSAT\_C, from several distant stations equipped with the TREMORS algorithm for seismic detection and analysis. The phase information, whose interpretation requires a precise knowledge of the epicenter-origin time combination, is not used. We carry out a direct inversion of Rayleigh and Love waves in the 90-300s period range with a control on the signal-to-noise ratio for each spectral amplitude. Estimates of focal depths, scalar moments and focal geometries obtained from the application of this simple method compare favorably with the solutions published using standard inversion procedures by the Harvard and USGS groups. This method, which allows the retrieval of focal geometry and scalar moment within one hour of origin time, holds great promise as an economical ingredient of tsunami warning systems.

**1. Introduction: The TREMORS System and INMARSAT-C Satellites**

In this paper, we present a method of seismic moment tensor inversion of mantle waves, using depleted datasets consisting of spectral amplitudes from as few as 3 to 4 stations. We are of course motivated by the desire to obtain a comprehensive picture of the source of a major, potentially tsunamigenic earthquake from the kind of restricted dataset that can be realistically accessed from a central laboratory in real time. We call this algorithm the Preliminary Determination of Focal Mechanism (or *PDFM*) method.

TREMORS (*T*sunami *R*isk *E*valuation through seismic *M*oment in a *R*eal time *S*ystem) is an integrated system based on a single three-component long-period seismic station linked to a

PC Type computer. Appropriate software automatically detects and analyzes the signals, providing a real-time estimate of the epicenter and of the scalar seismic moment, obtained from the computation of the mantle magnitude  $M_m$ , via  $\log M_0 = M_m + 13.0$ , where  $M_0$  is in N.m. We refer the reader to Okal and Talandier [1989, 1990] for details of the computation of  $M_m$ , and to Reymond et al. [1991], Hyvernaud et al. [1992], Schindel  et al. [1995] and Reymond et al. [1996] for technical descriptions of TREMORS.

The system is also capable of issuing alarms and early warnings and of sending them via INMARSAT-C satellite communications, together with a limited amount of seismic data and parameters. Typically, the former would consist of spectral amplitudes of the ground motion of Rayleigh and Love waves, computed at selected mantle frequencies in the range 3-20 mHz (50-300 s), as well as relevant information on background noise. The latter would include one-station epicentral estimates based on  $S$ - $P$  arrival times and 3-D reconstruction of  $P$ -wave ground motion [Reymond et al., 1991]. Such information amounts to no more than a few tens of numbers, which can be sent efficiently and economically to a central receiving location within the hour following the origin time of the earthquake. The surface wave spectral data are then ready to be inverted. By using exclusively spectral amplitudes, we ignore the phase information, whose interpretation requires an accurate knowledge of the earthquake epicenter and origin time, of which only rough estimates may be available in real time. On the other hand, and as discussed below, the solution obtained suffers in general from a two-fold indeterminacy, which, however, can usually be lifted from an examination of the general geological context of the event. This matter is discussed in some detail by Romanowicz and Su rez [1983]. Figure 1 shows the layout of the network used in the present study, the main station being located at the Geophysical Laboratory in Papeete, Tahiti (PPT). Because of operational developments, not all nine stations were simultaneously available, and the particular examples detailed below involved only 5 and 4 stations, respectively.

## 2. Methodology: A two-stage approach

The inversion for the moment tensor is carried out in two stages. In the first one, we seek to determine the focal depth, as well as a preliminary estimate of the azimuth of a focal plane, by constraining *a priori* the nature of the focal mechanism; in the second stage, we then use the resulting parameters as a starting model for a complete inversion of the moment tensor from the dataset of both Love and Rayleigh spectral amplitudes.

### a) First stage of the inversion

We use the method developed by Romanowicz [1981], itself composed of two steps, and involving the non-linear inversion of Rayleigh wave spectral amplitudes. This method is described in detail by Romanowicz [1982], Romanowicz and Su rez [1983] and Romanowicz and Guillemant [1984].

Using the formalism of Kanamori and Stewart [1976] and Kanamori and Given [1981], the modulus of the Rayleigh wave spectrum at angular frequency  $\omega$ , for a station located at an azimuth  $\theta$  from a source at depth  $h$ , can be expressed as a function of the components  $M_{kl}$  of the moment tensor through :

$$R(\omega, h) = \sqrt{R_r^2(\omega, h) + R_l^2(\omega, h)}$$

where  $R_r$  and  $R_i$  are the real and imaginary parts of the Rayleigh wave spectrum :

$$\begin{aligned} R_r(\omega, h) &= \frac{1}{2} M_{zz} S_R(\omega, h) + \frac{1}{2} (M_{yy} - M_{xx}) P_R(\omega, h) \cos 2\theta - P_R(\omega, h) M_{xy} \sin 2\theta \\ R_i(\omega, h) &= M_{xz} Q_R(\omega, h) \cos \theta + M_{yz} Q_R(\omega, h) \sin \theta \end{aligned} \quad (1)$$

Here,  $S_R$ ,  $P_R$ ,  $Q_R$  are excitation functions depending only on source depth and frequency, for a given structural model of the source region. In (1), we have assumed a deviatoric source involving no change of volume ( $\sum M_{ii} = 0$ ), and we have ignored the dependence on distance  $\Delta$  due to geometrical spreading and anelastic attenuation, both of which are independent of focal geometry and depth. As a preliminary step, a distance correction is performed for each observed spectral amplitude, using a regionalized dispersion model, as discussed by Okal and Talandier [1989].

When considering a set of observations at several stations (indexed  $j$ ) at azimuths  $\theta_j$ , Equations (1) can be rewritten as a function of five coefficients,  $A_i$ ,  $B_i$ ,  $C_i$ ,  $D_i$ ,  $E_i$  at each angular frequency  $\omega_i$  :

$$R_{ij}^2 = (A_i \sin 2\theta_j + B_i \cos 2\theta_j)^2 + (D_i \sin \theta_j + E_i \cos \theta_j)^2 \quad (2)$$

where

$$\begin{aligned} A_i &= -P_R(\omega_i, h) M_{xy} \\ B_i &= \frac{1}{2} P_R(\omega_i, h) (M_{yy} - M_{xx}) \\ C_i &= \frac{1}{2} S_R(\omega_i, h) M_{zz} \\ D_i &= Q_R(\omega_i, h) M_{xz} \\ E_i &= Q_R(\omega_i, h) M_{yz} \end{aligned} \quad (3)$$

In the first step of Romanowicz' [1982] method, Equations (2) are solved at each frequency for the coefficients (3), this procedure being non-linear. Then, in the second step, Equations (3) are solved for the tensor elements  $M_{kl}$  through a linear least-squares algorithm. Focal depth is estimated by carrying out several inversions at distinct constrained focal depths, and retaining the depth optimizing the variance reduction.

When working with very small datasets (in practice, 3 to 6 stations), a number of difficulties arise regarding the singularity of the resolving kernels in the inversion. In particular, it is well known that the dip-slip moment tensor components  $M_{xz}$  and  $M_{yz}$  have excitation coefficients  $Q_R$  vanishing for asymptotically shallow source depths, which leads to instabilities in unconstrained moment tensor inversions, especially when focal depth is left to float. For this reason, we impose (in this step alone)  $M_{xz} = M_{yz} = 0$ , thus reducing the number of unknowns to 3. In doing so, previous workers [e.g., Kanamori and Given, 1981] have shown that the inversion becomes generally very stable, and that the estimates of focal depth and strike azimuth  $\phi$  remain robust. The focal mechanisms estimated from this first stage in the procedure

are of course constrained to being pure strike-slip ( $\delta = 90^\circ$ ;  $\lambda = 0$  or  $180^\circ$ ) or pure thrust or normal faulting ( $\delta = 45^\circ$ ;  $\lambda = 90$  or  $270^\circ$ ).

**b) Second stage of the inversion:**

Once focal depth has been estimated, we proceed with a full inversion for the five moment tensor elements of the dataset of spectral amplitudes in (1), complemented by their Love wave analogs, as given by:

$$|L(\omega)|^2 = [P_L (M_{yy} - M_{yx}) \sin 2\theta + P_L M_{xy} \cos 2\theta]^2 + [Q_L (M_{yz} \cos \theta - M_{xz} \sin \theta)]^2 \quad (4)$$

Equations (2) and (4) are combined into a general non-linear system in which the  $M_{ki}$  are the unknowns. In practice, if the available dataset consists of 10 periods (from 100 s to 300 s), sampled for Rayleigh and Love waves at five stations, we have to solve 100 equations for 5 unknowns. These non-linear equations are solved iteratively, after injecting a trial solution (in practice, the output from Stage 1). In general, when the inversion is stable and the system well-behaved, the geometry of the trial solution has little if any influence on the final result. However, Stage 1 remains crucial for constraining source depth.

Equations (1) and (4) show that using only the modulus of the spectra results in a two-fold indeterminacy. First, the sense of slip on the fault plane can be reversed (the corresponding sources would have similar strike and dip but slip  $\lambda$  differing by  $180^\circ$ ; as a result, all spectral phases would differ by  $\pi$ ). Also, the entire solution can be rotated  $180^\circ$  in the horizontal plane (the corresponding solutions would have similar dip and slip, but the strike  $\phi$  would differ by  $180^\circ$ ; all spectral phases would be changed to their complex conjugate). This indeterminacy can potentially be removed by the combination of the observation of a  $P$ -wave polarity and of the interpretation of the probable geological context of the earthquake.

More complete and classical methods of moment tensor inversion use the full complex spectrum and interpret the phase information following a path correction. The latter requires an accurate knowledge of both the exact epicenter-origin time combination, and of the phase velocity along the path (to a typical accuracy of 0.5% [Aki and Patton, 1978]). In this respect, a significant advantage of our method is that we do not need a particularly accurate source location (in practice  $\pm 400$  km). This was verified in a series of tests by artificially moving the epicenter before performing the inversion.

**Source finiteness: Duration and Directivity.**

The previous formalism assumed that the seismic source could be modeled as a point source in space and time. As the earthquake size grows, this assumption can become unwarranted at the frequencies used in the inversion, and source finiteness thus has to be taken into account. In very simple terms, scaling laws [Geller, 1976; Kanamori and Given, 1981] predict that the source duration,  $\tau$ , grows linearly with the length of rupture  $L$ , while the seismic moment  $M_0$  grows as  $L^3$ , suggesting the following relation between  $\tau$  and  $M_0$ :

$$\tau = 4.8 \cdot 10^{-6} M_0^{1/3} \quad (5)$$

where  $\tau$  is in s and  $M_0$  in N.m. This relation corresponds to a rupture velocity of approximately 3.45 km/s, and is used by the Harvard CMT program to describe the source duration of small earthquakes for which it cannot be independently resolved by the inversion algorithm. The effect of source finiteness on the spectral amplitude of a surface wave has been described by Ben-Menahem [1963] as a multiplicative factor known as the directivity function:

$$F(\omega) = \frac{\sin X}{X} \exp(-iX)$$

with  $X = \frac{\omega L}{2V} - \frac{\omega L}{2C} \cos(\phi_S - \phi_R)$  where  $L$  is the fault length,  $V = L/\tau$  is the rupture velocity,  $C$  is the phase velocity at angular frequency  $\omega$ ,  $\phi_S$  is the station azimuth as measured from the fault strike, and  $\phi_R$  is the azimuth of rupture as measured from the fault strike. In practice,  $\phi_R$  is taken as 0. The effect of directivity is that of a low-pass filter depending on azimuth. At each step of the iteration, the value of the scalar moment is recomputed, an estimate of  $\tau$  is obtained, and the spectral amplitudes  $R_{ij}$  and  $L_{ij}$  are corrected for the appropriate values of  $|F|$  before proceeding with the inversion.

### 3. Examples of inversion for source parameters

In this section, we document our method in some detail on the examples of the two Peruvian events of 21 February 1996 in Chimbote and 12 November 1996 in the Nazca Province. The Chimbote earthquake was accompanied by a very significant, meter-scale, tsunami, and featured a source slowness characteristic of the so-called "tsunami earthquakes" [Tanioka et al., 1996; Newman and Okal, 1998]. The Nazca earthquake was of generally similar size, but its tsunami reached only a maximum amplitude of 35 cm.

As shown on Figure 2, we had available five stations for the Chimbote event, and only four for the Nazca one. We used first passages of both Love and Rayleigh waves. Results are given on Figures 3 and 4. In each of them, the lower right frame illustrates the determination of focal depth by Stage 1 of the inversion. The mechanisms inverted in Stage 2 are given in the lower left frames. The upper frames give the USGS and Harvard solutions for comparison. Note that the depth of the Chimbote event is best modeled at 20 km, with a relatively flat residual curve providing only coarse resolution, while the Nazca event has a much better resolved and greater depth of 45 km. These results are in good agreement with the Harvard depths (constrained at 15 km for Chimbote, inverted at 37 km for Nazca), and with the respective tsunamis of the two events. The focal geometries resulting from our inversions are also in excellent agreement with the published mechanisms (a quantification of this agreement is discussed in the next section). The inverted scalar moments match the Harvard ones very well; in the case of the slow Chimbote event, and not unexpectedly, the USGS moment, computed from higher-frequency body waves, remains deficient by roughly a factor of 2. Finally, it is worth emphasizing that this study used data from only 5 and 4 stations, respectively, while in the case of the Chimbote event for example, the Harvard and USGS solutions were achieved with 62 and 51 stations respectively.

#### 4. Application to an enhanced dataset and discussion

We have applied systematically the above method to a dataset of 17 strong earthquakes (including two at intermediate depths), spanning the time interval January 1996-March 1998, and listed in Table 1. Results are shown on Figure 5. In order to assess the performance of the method, we examine here independently the three source parameters obtained in the inversion: focal depth, focal geometry, and scalar moment.

##### *1. Focal depth*

Focal depth estimates are presented in Figure 6, in the form of a direct plot against Harvard-inverted depths. For reference, USGS depths are also plotted. It is immediately evident that PDFM depths generally match the Harvard ones very well, and in particular better than do the USGS-inverted depths.

##### *2. Focal Geometry*

A representative set of focal geometries inverted by the three methods (PDFM; USGS and Harvard) is presented in Figure 5. The agreement between the several methods is generally good and can be further assessed quantitatively by computing the quantity

$$f = \sqrt{(\mathbf{P}_i \cdot \mathbf{P}_k)(\mathbf{T}_i \cdot \mathbf{T}_k)} \quad (6)$$

which measures the angular distance between two solutions (indexed  $i$  for the published geometry and  $k$  for the reference one) by taking the product of the direction cosines between their respective tension and pressure axes,  $\mathbf{P}$  and  $\mathbf{T}$  ( $f$  would be 1 if the two solutions were identical, and 0 if any two principal directions were exchanged between solutions). Figure 7 shows the values of  $f$  for the 17 earthquakes studied, computed using both the Harvard (dark stippled bars) and USGS (light dotted bars) mechanisms as reference. The good performance of the PDFM method relative to the Harvard geometries is confirmed, with values of  $f$  always greater than 0.7, and generally than 0.8.

##### *3. Scalar Moment*

Finally, as discussed previously, notably by Talandier and Okal [1989], the scalar moment remains the quantitative parameter of choice for far-field tsunami generation, and hence the most important one in the context of tsunami warning. In practice, a threshold of  $M_0 \geq 10^{20}$  N.m, seems adequate for most regionally destructive tsunamis (at distances of 1 to a few hundred km)<sup>1</sup> and  $M_0 \geq 5.0 \cdot 10^{21}$  N.m for catastrophic destructive trans-oceanic tsunamis (at distances of 1 to several thousand km), this being the range of the truly giant and exceptional earthquakes. Figure 8 shows that our estimates of  $M_0$  are generally very close to the ones published by Harvard, often times more so than the USGS values. In particular, we correctly assess such anomalous events as the Chimbote "tsunami earthquake", which the

<sup>1</sup> At shorter distances, on the order of a few km to a few tens of km, this threshold should be lowered, as evidenced by the recent Sandaun, Papua New Guinea, event of 17 July 1998. The feasibility of any kind of tsunami warning at such short distances remains elusive.

USGS inversion underestimates substantially (by a factor of 2.5). In cases when discrepancy is present between the PDFM and Harvard geometries (e.g., Solomon Islands, 29 April 1996), it involves a slight rotation of one of the mechanism angles, but the general character of the solution is adequate. In particular, when the Harvard and USGS mechanisms differ strongly (e.g., Santa Cruz, 21 April 1997), the PDFM geometry mirrors the Harvard CMT. Thus, inferences on the tsunamigenic potential of the earthquake would not be utterly sensitive to the difference in mechanism with the Harvard solution.

This good level of performance of our method, when compared to the Harvard inversions, had to be expected to some extent, in that our measurements of  $M_0$  utilize mantle surface waves and are thus fundamentally low-frequency in nature, as opposed to the higher-frequency body wave inversions carried out by the USGS. Furthermore, the PDFM method can be regarded as a refinement of the general concept of the magnitude  $M_m$ , whose excellent performance as an estimator of scalar moment has been amply described in previous publications [Okal and Talandier, 1989; Hyvernaud et al., 1992].

### Conclusion

In conclusion, the PDFM method which we have developed to estimate the moment tensor of the source of a distant earthquake based on restricted datasets, shows very promising results with obvious applications to tsunami warning. Our ultimate goal would be to provide an estimate of the moment tensor in the hour following the origin time of the earthquake; this goal is attainable, but will require progress in further automation, particularly in the field of data selection. In addition, the PDFM method has an interesting potential for application to historical earthquakes, for which datasets are occasionally very depleted, and time corrections unavailable, making it impossible to correctly utilize the phase information, especially when dealing with several stations whose clocks may be asynchronous, as discussed by Huang et al. [1994].



Table 1.: Events used in this study

Region	Date	Origin time	$M_0$ (USGS)	$M_0$ (Harvard)	$M_0$ (PDFM) <i>This Study</i>
Kuril Islands	07 Feb. 1996	21:36:45	0.48	0.64	0.67
Biak, Irian-Jaya	17 Feb. 1996	05:59:30	18	24	29
Chimbote, Peru	21 Feb. 1996	12:51:04	1.1	2.2	1.9
Mexico	25 Feb. 1996	03:08:19	0.54	0.55	0.80
Solomon Islands	29 Apr. 1996	14:40:41	0.48	0.76	0.80
Aleutian Islands	10 Jun. 1996	15:24:56	7.3	8.6	9.1
Nazca, Peru	12 Nov. 1996	16:59:44	3.7	4.4	3.0
Santa Cruz	21 Apr. 1997	12:02:26	2.3	5.7	5.5
Chile	15 Oct. 1997	01:33:33	0.52	0.43	0.55
Peru	28 Oct. 1997	06:15:17	0.67	0.76	0.64
Sulawesi	25 Nov. 1997	12:14:33	0.50	0.36	0.45
Kamchatka	05 Dec. 1997	11:26:54	3.9	6.8	4.4
Loyalty Islands	04 Jan. 1998	06:11:59	1.2	1.6	2.2
Fiji Islands	12 Jan. 1998	16:36:20	0.12	0.11	0.25
Chile	30 Jan. 1998	12:16:08	0.37	0.39	0.45
North Atlantic	16 Feb. 1998	23:53:20	0.14	0.15	0.14
Balleny Islands	25 Mar. 1998	03:12:25	4.6	17	15

Seismic moments are given in units of  $10^{20}$  dyn-cm.

## REFERENCES

- Aki, K., and Patton, H., 1978, Determination of moment tensor using surface waves, *Tectonophysics*, **49**, 213-222.
- Ben-Menahem, A., 1961, Radiation of seismic surface waves from finite moving sources, *Bull. Seismol. Soc. Amer.*, **51**, 401-435.
- Geller, R.J., 1976, Scaling relations for earthquake source parameters and magnitudes, *Bull. Seismol. Soc. Amer.*, **66**, 1501-1523.
- Huang, W.-C., Ekström, G., Okal, E.A., and Salganik, M.P., 1994, Application of the CMT algorithm to analog recordings of deep earthquakes, *Phys. Earth Planet. Inter.*, **83**, 283-297.
- Hyvernaud, O., Reymond, D., Talandier, J., and Okal, E.A., 1993, Four Years of Automated Measurement of Seismic Moments at Papeete using the Mantle Magnitude  $M_m$ : 1987-1991, *Tectonophysics*, **217**, 175-193.
- Kanamori, H., and Given, J.W., 1981, Use of long-period surface waves for rapid determination of earthquake-source parameters, *Phys. Earth Planet. Inter.*, **27**, 8-31.
- Kanamori, H., and Stewart, G.S., 1976, Mode of strain release along the Gibbs Fracture Zone, *Phys. Earth Planet. Inter.*, **11**, 312-332.
- Newman, A.V., and Okal, E.A., 1998, Teleseismic estimates of radiated seismic energy: The  $E/M_0$  discriminant for tsunami earthquakes, *J. Geophys. Res.*, in press.
- Okal, E.A., and Talandier, J., 1989,  $M_m$ : A variable-period mantle magnitude, *J. Geophys. Res.*, **94**, 4169-4193.
- Okal, E.A., and Talandier, J., 1990,  $M_m$ : Extension to Love waves of the concept of a variable-period mantle magnitude, *Pure Applied Geophys.*, **134**, 355-384.
- Reymond, D., Hyvernaud, O., and Talandier, J., 1991, Automatic detection, location and quantification of earthquakes: Application to Tsunami Warning, *Pure Applied Geophys.*, **135**, 361-382.
- Reymond, D., Robert, S., Thomas, Y., and Schindelé, F., 1996, An automatic tsunami warning system: TREMORS; Application in Europe, *Phys. Chem. Earth*, **21**, 75-81.

**Romanovicz, B.A., 1981,** Depth resolution of earthquakes by moment tensor inversion of long period Rayleigh waves, Effects of phase velocity variations across Eurasia, *J. Geophys. Res.*, **86**, 5963-5984.

**Romanovicz, B.A., 1982,** Moment tensor inversion of long period Rayleigh waves: a new approach, *J. Geophys. Res.*, **87**, 5395-5407.

**Romanovicz, B.A., and Guillemant, P., 1984,** An experiment in the retrieval of depth and source mechanism of large earthquakes using very long-period Rayleigh wave data, *Bull. Seism. Soc. Amer.*, **74**, 417-437.

**Romanovicz, B.A., and Suárez, G., 1983,** On an improved method to obtain the moment tensor and depth of earthquakes from the amplitudes spectrum of Rayleigh waves, *Bull. Seism. Soc. Amer.*, **73**, 1513-1526.

**Schindelé, F., Reymond, D., Gaucher, E., and Okal, E.A., 1996,** Analysis and automatic processing in near field of eight 1992-1994 tsunamigenic earthquakes: improvements towards real-time tsunami warning, *Pure Applied Geophys.*, **144**, 381-408.

**Talandier, J., and Okal, E.A., 1989,** An algorithm for automated tsunami warning in French Polynesia based on mantle magnitude, *Bull. Seism. Soc. Amer.*, **79**, 1177-1193.

**Tanioka, Y., Ruff, L.J., and Satake, K., 1996,** The recent large tsunamigenic earthquakes, *Eos, Trans. Amer. Geophys. Un.*, **77**, (17), S184 [abstract].

**Figure 1:** Map of TREMORS stations used in this study. Each station is equipped with a 3-component long-period broad-band seismometer linked to a PC-type computer. The events are automatically detected and analysed. The results, including location, phase arrival times, spectral amplitudes and estimates of the mantle magnitude  $M_m$ , make up a dataset of a few tens of parameters, which are sent within the hour by INMARSAT\_C satellite to the central receiving station at Papeete (PPT).

**Figure 2:** Examples of inversions for the two Peruvian earthquakes of 21 February 1996 (Chimbote) and 12 November 1996 (Nazca). The maps show the five TREMORS stations used in the inversions, and the azimuthal coverage, as documented by the great circle paths involved.

**Figure 3:** Chimbote, Peru, event of 21 February 1996. This figure compares the solutions published by Harvard and the USGS (top frames) with those obtained in the present study (bottom left). The diagram at bottom right illustrates the resolution of focal depth by plotting the r.m.s. residuals of the first stage of inversion as a function of constrained depth. See text for details.

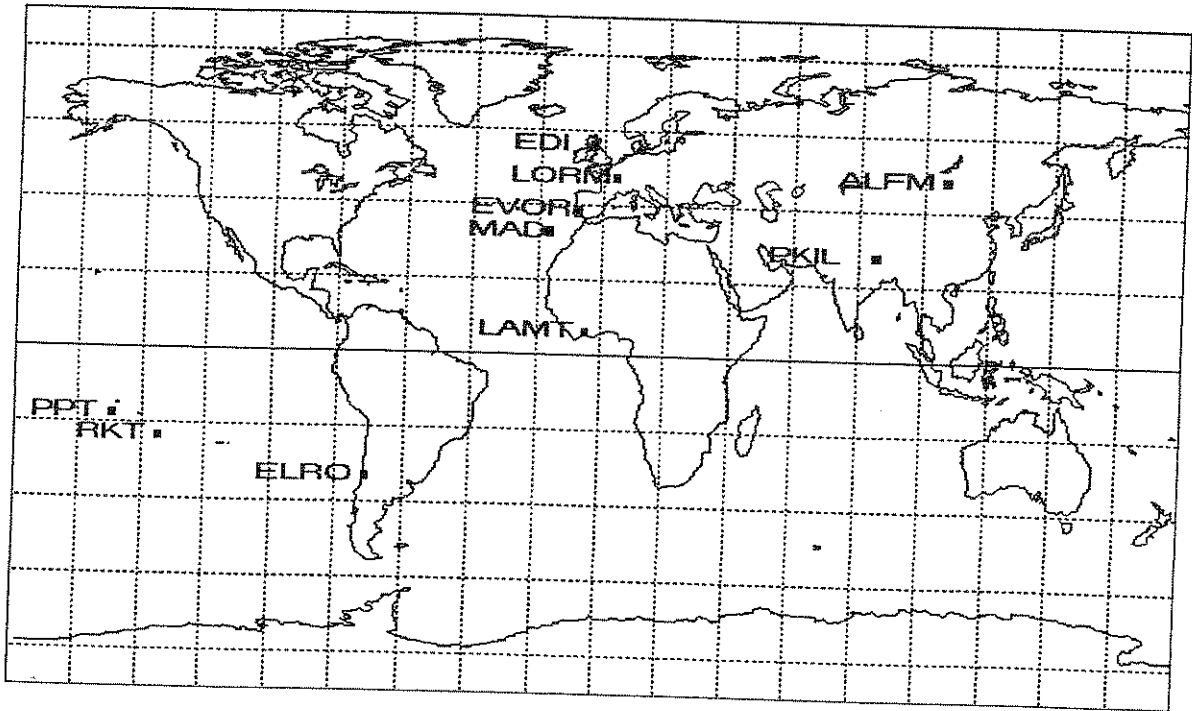
**Figure 4:** Same as Figure 3 for the Nazca, Peru, event of 12 November 1996. Note in particular the depth discrepancy between the Harvard and USGS depths.

**Figure 5:** Results of inversion for 17 events listed in Table 1. *Top:* USGS solutions; *Center:* Harvard solutions; *Bottom:* PDFM solutions (this study).

**Figure 6:** Comparison of focal depths obtained in the enhanced study (solid squares; 17 events) with the Harvard CMT depths. The PDFM depths are generally very comparable to Harvard values; on the other hand, the USGS inversion (dots) has a tendency to underestimate depth, as compared to Harvard.

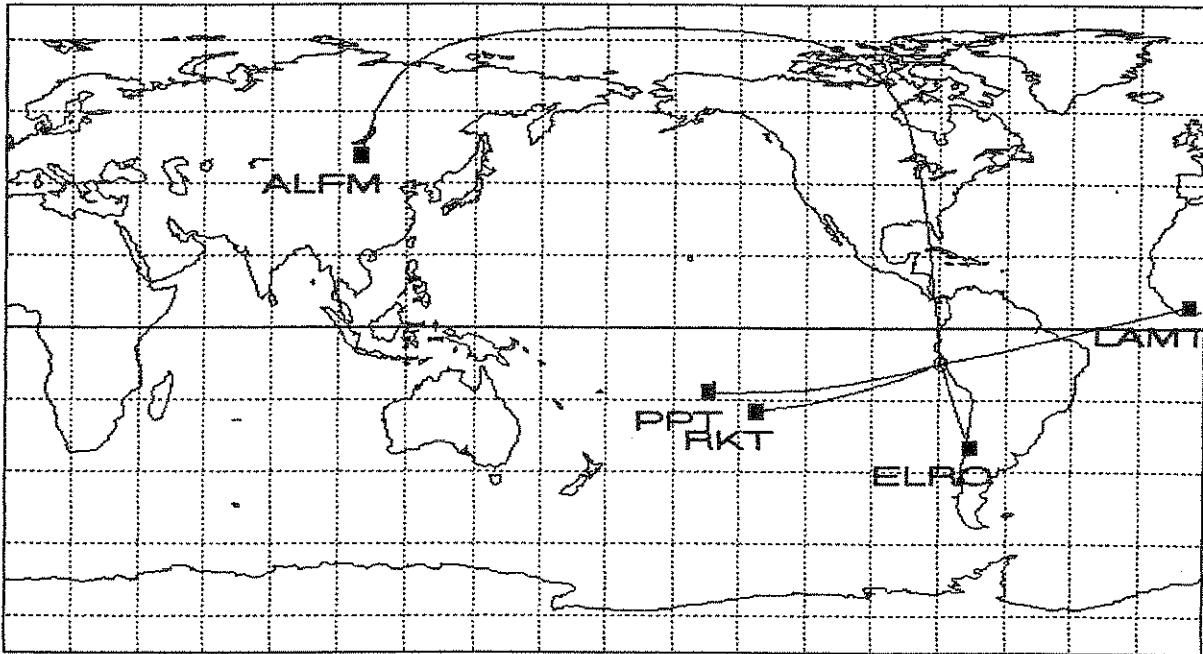
**Figure 7:** Comparison of focal geometries achieved with the three methods. For each of the 17 events studied, the light, dotted vertical bar rises to the value of the function  $f$  defined by (6) for the Harvard mechanism taken as the reference ( $k$ ). The stippled dark bar similarly compares our solution to the USGS one.

**Figure 8:** PDFM scalar moments (solid squares) plotted as a function of published Harvard moments. Note the generally excellent fit, and the absence of systematic trend in the residual as a function of size. For reference, the USGS moments are also shown (dots). Note that they exhibit a systematic negative residual with respect to the Harvard values.

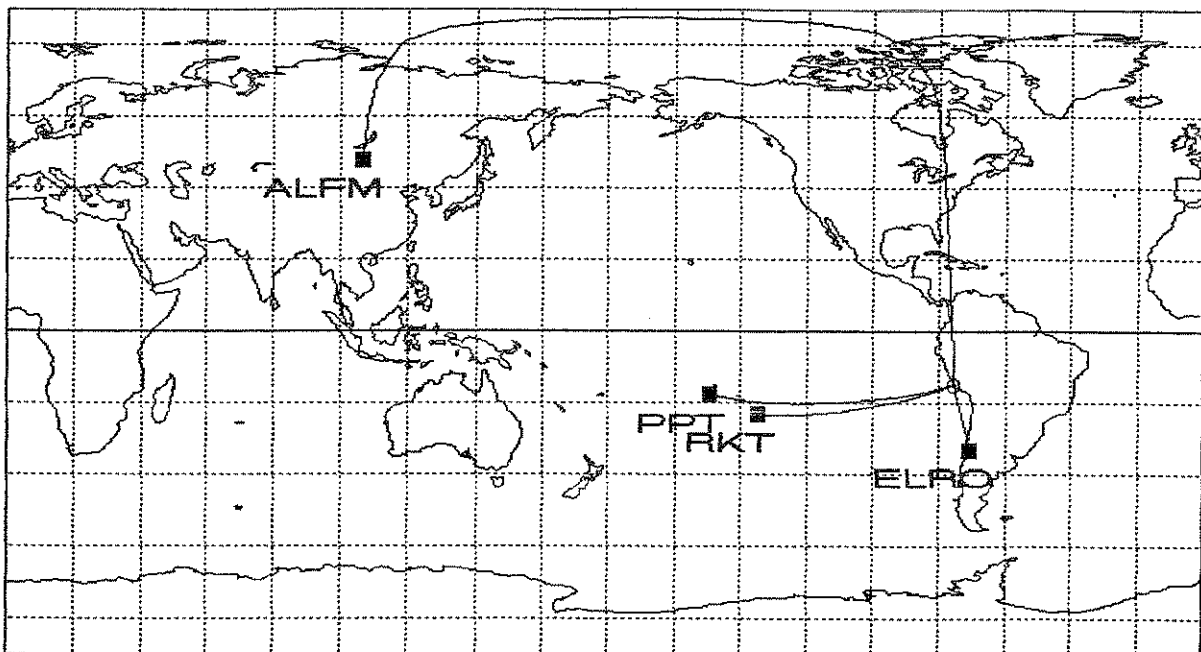


**Figure 1:** Map of TREMORS stations used in this study. Each station is equipped with a 3-component long-period broad-band seismometer linked to a PC-type computer. The events are automatically detected and analysed. The results, including location, phase arrival times, spectral amplitudes and estimates of the mantle magnitude  $M_m$ , make up a dataset of a few tens of parameters, which are sent within the hour by INMARSAT\_C satellite to the central receiving station at Papeete (PPT).

## Chimbote, Peru, 21 Feb. 1996

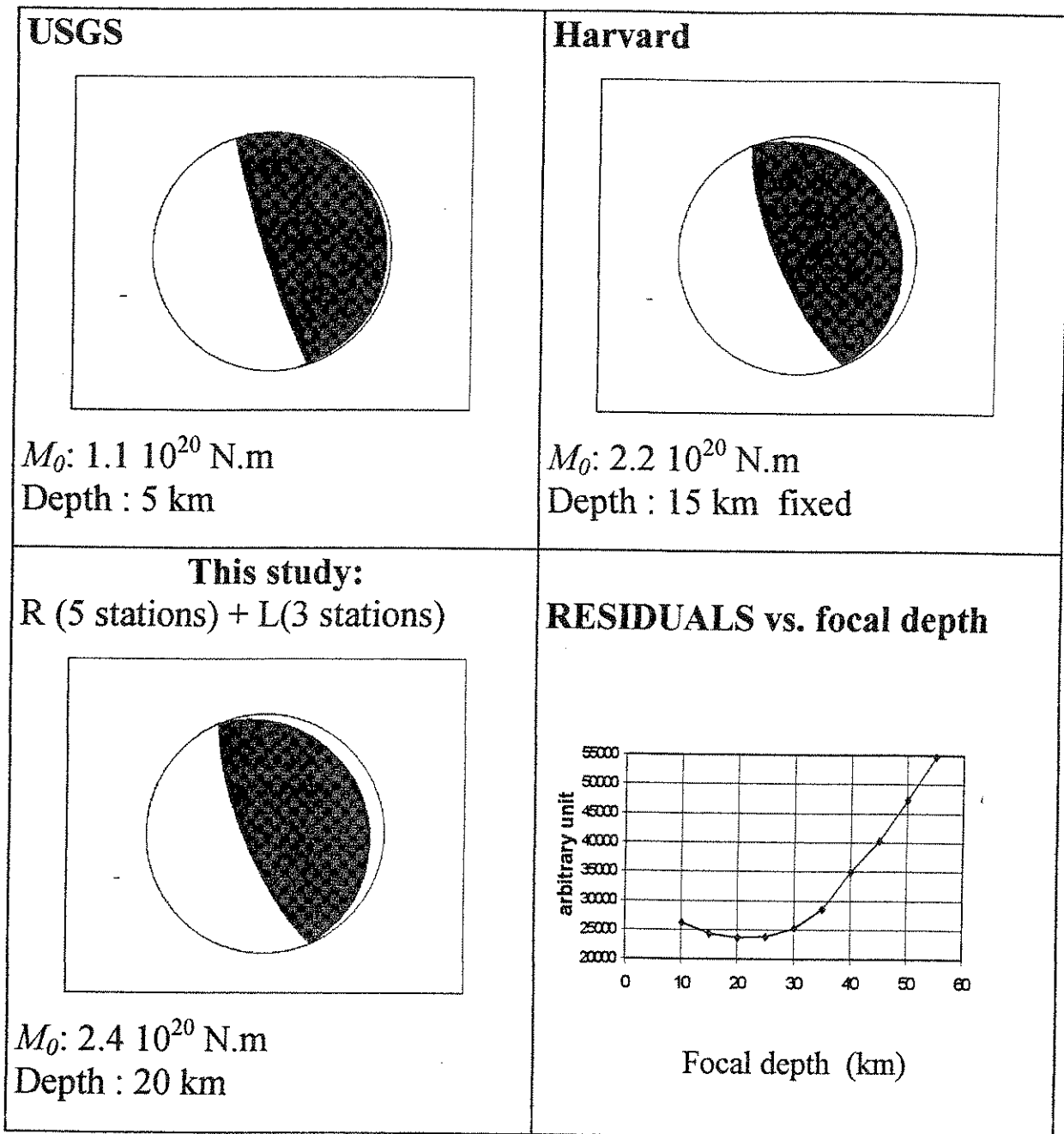


## Nazca, Peru, 12 Nov. 1996



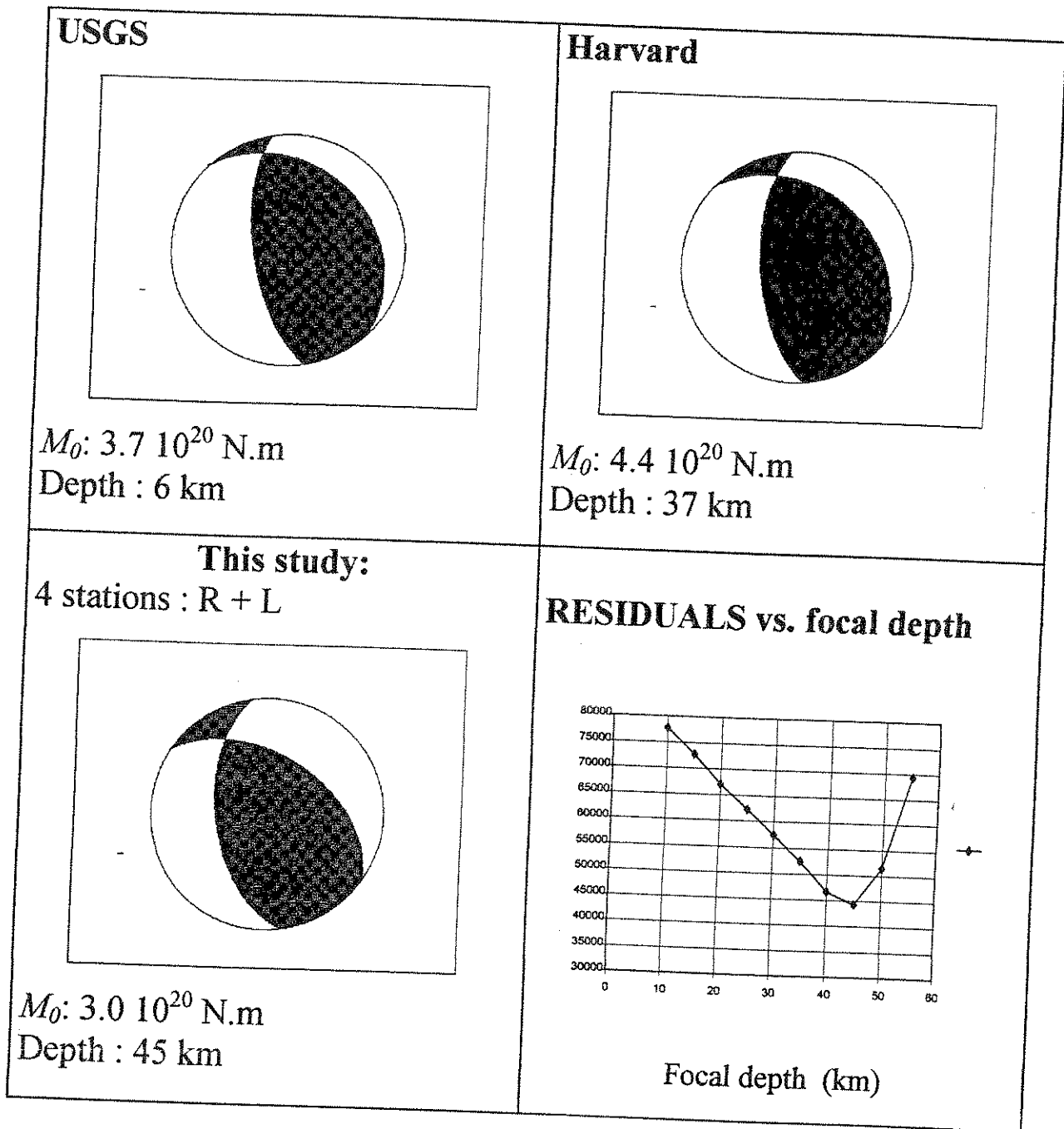
**Figure 2:** Examples of inversions for the two Peruvian earthquakes of 21 February 1996 (Chimbote) and 12 November 1996 (Nazca). The maps show the five TREMORS stations used in the inversions, and the azimuthal coverage, as documented by the great circle paths involved.

# Chimbote, Peru, 21 February 1996



**Figure 3:** Chimbote, Peru, event of 21 February 1996. This figure compares the solutions published by Harvard and the USGS (top frames) with those obtained in the present study (bottom left). The diagram at bottom right illustrates the resolution of focal depth by plotting the r.m.s. residuals of the first stage of inversion as a function of constrained depth. See text for details.

Nazca, Peru, 12 November 1996



**Figure 4:** Same as Figure 3 for the Nazca, Peru, event of 12 November 1996. Note in particular the depth discrepancy between the Harvard and USGS depths. .



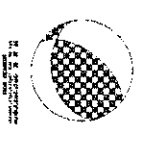
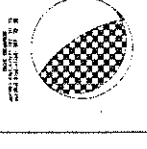

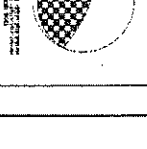
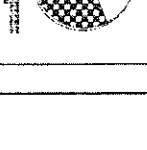
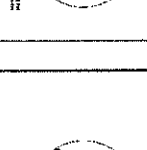

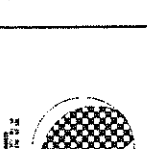

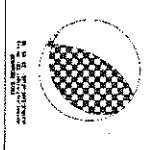
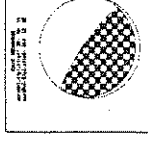
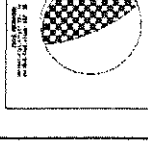
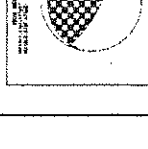
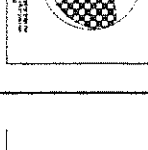
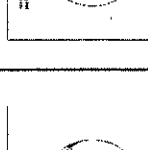
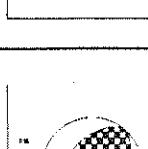
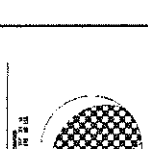
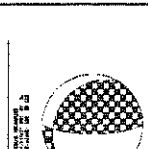
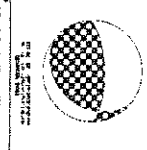
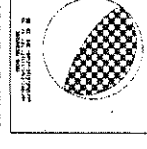
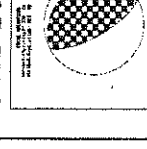
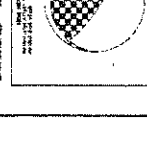
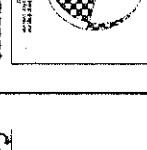
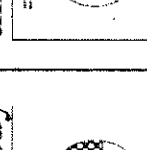
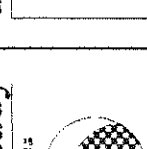
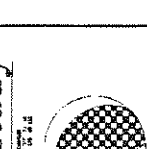
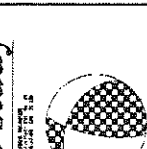
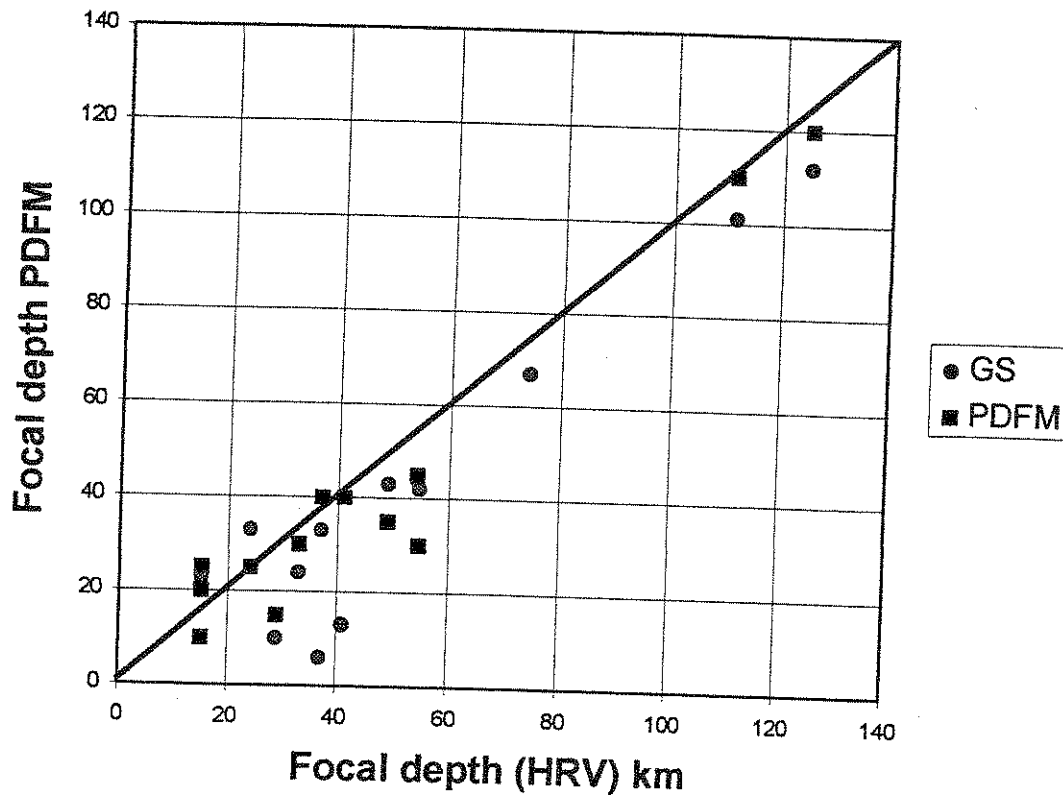
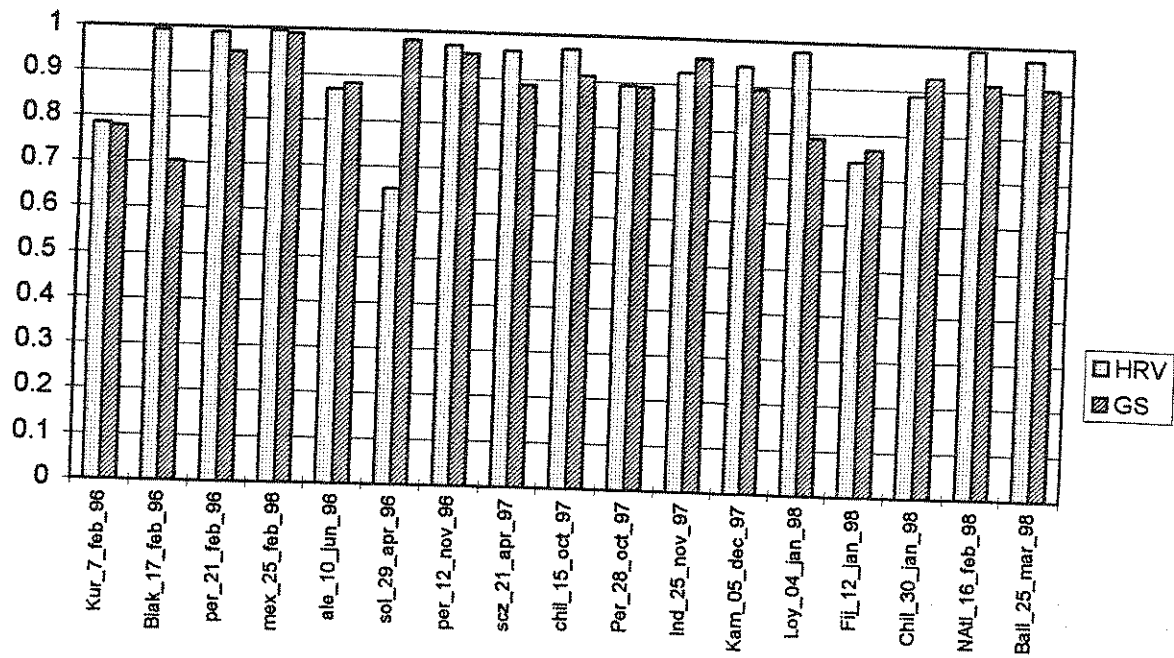
USGS 	USGS 	USGS 	USGS 	USGS 	USGS 	USGS 	USGS 	USGS 
Harvard 	Harvard 	Harvard 	Harvard 	Harvard 	Harvard 	Harvard 	Harvard 	Harvard 
this study 	this study 	this study 	this study 	this study 	this study 	this study 	this study 	this study 
Kuril 07 FEB 96	Biak 17 FEB 96	Peru 21 FEB 96	Mexico 25 FEB 96	Aleutian 10 JUN 96	Solomon 29 APR 96	Peru 12 NOV 96	Peru 12 NOV 96	Santa Cruz 21 APR 97

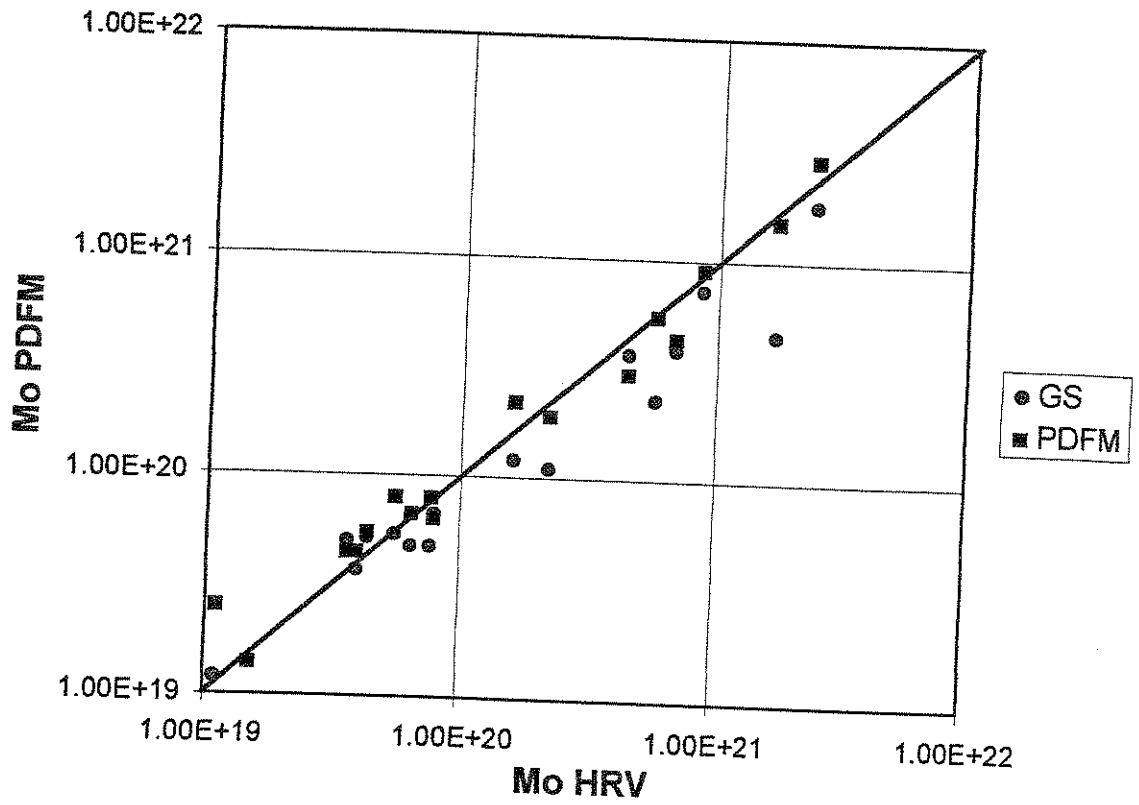
Figure 5: Results of inversion for 17 events listed in Table 1. Top: USGS solutions; Center: Harvard solutions; Bottom: PDFM solutions (this study)



**Figure 6:** Comparison of focal depths obtained in the enhanced study (solid squares; 17 events) with the Harvard CMT depths. The PDFM depths are generally very comparable to Harvard values; on the other hand, the USGS inversion (dots) has a tendency to underestimate depth, as compared to Harvard.



**Figure 7:** Comparison of focal geometries achieved with the three methods. For each of the 17 events studied, the light, dotted vertical bar rises to the value of the function  $f$  defined by (6) for the Harvard mechanism taken as the reference ( $k$ ). The stippled dark bar similarly compares our solution to the USGS one.



**Figure 8:** PDFM scalar moments (solid squares) plotted as a function of published Harvard moments. Note the generally excellent fit, and the absence of systematic trend in the residual as a function of size. For reference, the USGS moments are also shown (dots). Note that, they exhibit a systematic negative residual with respect to the Harvard values.